Energy
Advances

ROYAL SOCIETY
OF CHEMISTRY

PAPER

View Article Online
View Journal | View Issue

Check for updates

Cite this: *Energy Adv.*, 2022, **1**, 926

Carbon coated titanium dioxide (CC-TiO_2) as an efficient material for photocatalytic degradation

Rahul Kumar, *[ab] Raveena Choudhary,[c] Santa Kolay,[a] O. P. Pandey,[c] Kulvir Singh[c] and Parag Bhargava[a]

Received 1st October 2021,
Accepted 4th October 2022

DOI: 10.1039/d1ya00015b

rsc.li/energy-advances

TiO_2 is an efficient, cost effective, and common photocatalyst. But there are some technical issues with TiO_2 such as fast charge recombination, wide band gap, and low surface area of bulk TiO_2 which limit the practical application of TiO_2 photocatalysts. Carbon coating of TiO_2 is found to provide many advantages such as high absorptivity, high photocatalytic activity, stability of the anatase phase, *etc.* In the present study, carbon coated titanium dioxide (CC-TiO_2) is fabricated by colloidal processing using TiO_2 powder and sucrose followed by heat treatment in an argon atmosphere at different temperatures. Samples are characterized by powder X-ray diffraction, BET technique, Raman spectroscopy, field emission gun scanning electron microscopy (FEG-SEM) and field emission gun transmission electron microscopy (FEG-TEM), respectively. The photocatalytic activity of CC-TiO_2 is studied for cationic dyes (MB (methylene blue) and CV (crystal violet)). The sample heat treated at 800 °C shows the highest photocatalytic activity. This particular sample exhibited the lowest optical band gap compared with all other heat-treated samples.

1. Introduction

Photocatalytic processes are accepted as feasible solutions for treating environment pollutants, specifically various organic substances through photocatalytic degradation. The development of semiconductor photocatalysts has drawn much attention as one of the most important goals in materials science.[1–3] TiO_2 is one of the most explored photocatalytic materials due to its high photocatalytic activity, high stability, low cost and low toxicity.[4,5] A lot of research work has been done on the modification of TiO_2 in order to improve the catalyst's efficiency including co-catalysts, dye sensitization, metal particle loading, metallic doping and non-metallic doping.[6,7] The only disadvantage of TiO_2 is that it cannot be activated by visible light due to its higher optical band gap.[5–8] ZnO, Fe_2O_3, SnO_2, WO_3, ZnS, CdS, and $LiNbO_3$ are other photocatalysts but these are less active and attractive because of the various limitations associated with them.[9–21] On the other hand, carbon materials such as graphite, carbon black and graphitized materials have been used in heterogeneous catalysis particularly as supports for precious metal particles (Pt, Ru, Au, *etc.*). Nanostructured carbon materials such as carbon nanotubes, fullerenes, and graphene offer new opportunities in the field of heterogeneous catalysis.[22–25]

Different nanocarbon–TiO_2 systems such as carbon doped TiO_2 nanoparticles, CNT–fullerene– and graphene–TiO_2 composites have been used as photocatalysts due to their outstanding properties. The combination of carbonaceous nanomaterials and a TiO_2 photocatalyst provides an opportunity to cumulatively improve photocatalytic efficiency through three mechanisms including, improved absorption of visible light, better adsorption of pollutants and facile charge separation and transportation.[26] First, the adsorption properties of carbonaceous materials are remarkable, which can particularly enhance the concentration of organic pollutants on the surface of a catalyst.[27] The improved adsorption of dye molecules on a catalyst surface is an important contribution toward photocatalytic activity improvement which facilitates the interface reaction of photocatalysis.[28] Second, it is well-known that carbonaceous nanomaterials can enhance light absorption of TiO_2 in the visible light range compared to pure TiO_2.[29–32] This enhanced absorption was attributed to chemical bonding (Ti–O–C bonds) between carbonaceous materials and TiO_2.[33–35] Additionally, carbonaceous materials are stable, inexpensive, and environmentally friendly and also play the key role of an electron reservoir to conduct away the electrons from the electron–hole pairs of TiO_2 due to the excellent electron-storage capability, thereby improving the efficiency of charge separation in TiO_2.[36–40] Many methods have been used to synthesize carbon doped TiO_2 composites such as simple mixing, sol–gel[41], hydrothermal,[42] thermal oxidation, physical vapor

---

[a] *Department of Metallurgical Engineering and Materials Science, Indian Institute of Technology Bombay, Mumbai, 400076, India. E-mail: kumarrahul003@gmail.com*
[b] *Centre for Energy Studies, Indian Institute of Technology Delhi, New Delhi, 110016, India*
[c] *School of Physics and Materials Science, Thapar Institute of Engineering and Technology, Patiala, 147004, India*

deposition (PVD),[43] chemical vapour deposition (CVD)[44] and electrophoretic deposition (EPD).[45]

In the present study, carbon coated TiO_2 (CC-TiO_2) was synthesized by colloidal processing using TiO_2 powder and sucrose. The proposed method is a simple and cost-effective method to fabricate CC-TiO_2. Sucrose was used as a soluble carbon source and sucrose coated TiO_2 was heat treated in an argon atmosphere at different temperatures. Sucrose upon pyrolysis yields carbon that gets coated on the titanium dioxide particles surface. The photocatalytic activity of CC-TiO_2 heat treated at different temperatures was investigated for MB (methylene blue) and CV (crystal violet) with a low concentration.

2. Experimental

2.1. Synthesis of carbon coated titanium oxide (CC-TiO_2) samples

Titania slurry was made by using TiO_2 nano powder, (P25, Degussa), polyethylene glycol (M_w = 600) PEG-600 (Thomas Baker) and distilled water. Sucrose (GR-Merck) was added to the suspension containing 10 vol% ceramic (TiO_2) in an amount which upon decomposition at moderate temperature would yield carbon in the range of 8 wt% with respect to the ceramic. Zirconia grinding media (2–3 mm diameter) was added to the slurry and the ratio of the grinding media and titania powder was 1 : 1. The slurry was made in a polypropylene bottle and kept on a pot mill for about 24 h.[46,47]

After preparation of the slurry, it was cast in ring shaped plastic molds which were placed on a gypsum base plate. To reduce adhesion of the cast body to the molds, the inner surface of the plastic molds was coated with WD40 (WD Company). Cast samples (green body) were removed from the plastic molds after drying under ambient conditions for 36 hours followed by drying in an oven maintained at 50 °C for 24 h. The cast samples were crushed using a mortar pestle to make the sucrose coated TiO_2 powder.[48,49] The annealing of the powder was carried out in a flowing argon gas at different temperatures (600, 800, 900 and 1000 °C) with a heating rate of 2 °C min^{-1} followed by a dwell time of 2h at each temperature to pyrolyze sucrose. CC-TiO_2 powders were obtained after annealing at different temperatures.

2.2. Sample preparation for photocatalytic degradation

Photocatalytic degradation of cationic dyes MB and CV using CC-TiO_2 heat treated at different temperatures was studied. In typical experiments, 5 mg L^{-1} of MB and CV solutions were prepared. 100 mg L^{-1} of each of CC-TiO_2 were suspended in 100 mL of the aliquot. The suspension was stirred magnetically first in the dark for 30 minutes to ensure the completion of adsorption–desorption equilibrium. Furthermore, the exposure of visible light (Philips household CFL; 85W; intensity ~8900 lux) was carried out onto the suspension with continuous stirring. After an interval of 20 minutes, 3 mL of the solution was taken and centrifuged to separate the dye and catalyst. Thereafter, the concentration of dye solution was monitored using a UV-visible spectrophotometer (Hitachi U-3900H).

2.3. Characterization of the CC-TiO_2 samples

The CC-TiO_2 heat treated at different temperatures was characterized using different tools. XRD (Model-PANalytical X'Pert Pro multipurpose XRD) was used to analyze the crystalline components of CC-TiO_2 heat treated at different temperatures operating at 40 kV and 40 mA and measurements were recorded from a diffraction angle $2\theta = 10^\circ$ to 90°, with a total accumulation time of around 60 min. The Brunauer–Emmett–Teller (BET) specific surface area measurement was carried out using a BET instrument (Smart Sorb 92/93, Smart Instruments Co.) Raman spectroscopy (Model-Renishaw Invia Raman Microscope) was used to characterize the extent of defects in carbon coated titania (CC-TiO_2) heat treated at different temperatures. Raman spectra were recorded at room temperature using a 514 nm wavelength. The laser power used for the samples was 0.1 mW. The laser was focused through a microscope with a 50X objective. Raman spectra presented in this study correspond to the accumulation of 4 spectra recorded from 300 to 3500 cm^{-1} over 30 seconds. To analyze the morphology of CC-TiO_2 field emission electron gun scanning microscopy (FEG-SEM) (JEOL, JSM-7600F) and a field emission gun transmission electron microscope (FEG-TEM) (JEOL, JEM-2100F) were used. For FEG-TEM measurements, samples were sonicated in methanol media for 2 minutes and then one drop of the mixture was added directly on the copper grid. The grid with the powder droplets was kept overnight in a desiccator and were loaded into the transmission electron microscope by a double tilt holder for the high resolution FEG-TEM images. A UV-Vis spectrophotometer (Hitachi U-3900H) was used in the spectral range of 250–800 nm to measure the band gap of the CC-TiO_2 heat treated at different temperatures. The scan speed and sampling interval during the scan are 300 nm min^{-1} and 0.50 nm, respectively. The photocatalytic activity of the CC-TiO_2 heat treated at different temperatures is measured in terms of the degradation of cationic dyes MB and CV. The extents of MB and CV are monitored using a UV–vis spectrophotometer (Hitachi U-3900H).

3. Results and discussion

3.1 XRD, BET, Raman and morphological analysis of CC-TiO_2 samples

Fig. 1 shows the X-ray diffraction patterns of CC-TiO_2 heat treated at different temperatures. The diffraction peaks for the sample heat treated at 600 °C can be seen in Fig. 1 and all of the peaks appear in the positions corresponding to the anatase phase and no diffraction peak for the rutile phase is observed. The diffraction peaks in the samples heat treated at 800 and 900 °C were corresponding to the anatase phase. In addition, peaks such as (105), (211), (116), (220), (215) and (224) corresponding to the rutile phase of titanium dioxide were observed in samples heat treated at 800 and 900 °C.[50,51] Samples heat treated at 1000 °C are indexed as being the rutile phase.

It can be seen from Fig. 1 that the rutile phase appears at an annealing temperature above 800 °C and the anatase phase completely transforms to the rutile phase around 1000 °C.

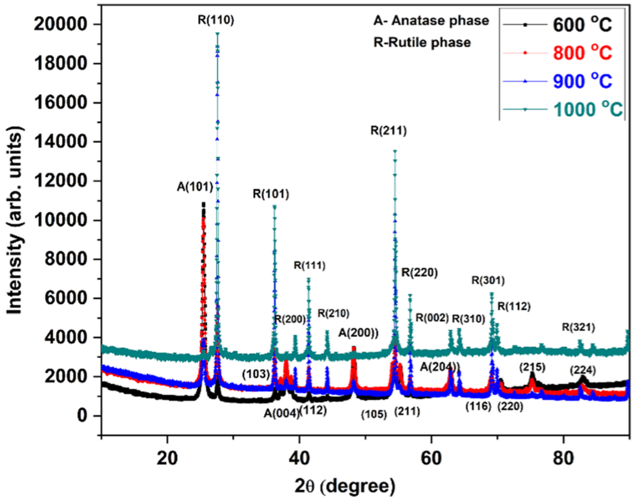

Fig. 1 XRD of CC-TiO$_2$ heat treated at different temperatures (600, 800, 900, and 1000 °C).

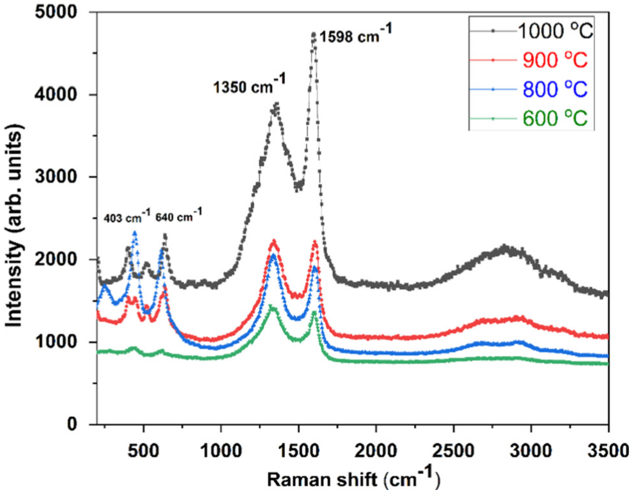

Fig. 2 Raman spectra of CC-TiO$_2$ heat treated at different temperatures (600, 800, 900, and 1000 °C).

For the sample heat treated at 1000 °C, the diffraction peaks of the anatase structure disappeared, and only the diffraction peaks of the rutile structure are observed.[52] Therefore, it is concluded that the anatase to rutile transformation occurred at a temperature above 800 °C and was completed at 1000 °C. Amores *et al.* reported that the crystal size of rutile formed by anatase phase transformation is always much larger.[53]

The rutile phase has a higher refractive index and ultraviolet absorptivity; thus, it has wide applications in pigments, paints, and ultraviolet absorbents. The anatase phase, on the other hand, is chemically and optically active, thus it is suitable for catalysts and a better choice for dye degradation.[54] For most catalytic reaction systems, it is generally accepted that anatase demonstrates a higher photocatalytic activity than rutile.[55] The crystallite size of CC-TiO$_2$ heat treated at different temperatures was determined using the Debye-Scherrer formula as given below.[50]

$$D = \frac{K\lambda}{\beta \cos\theta}$$

where D is the crystallite size, K is the shape factor, λ is the wavelength of X-ray radiation (Cu Kα = 1.5406 Å), β is full width at the half maximum (FWHM) after making appropriate base line correction and subtracting instrumental broadening, and θ is the diffraction angle.

The crystallite size of CC-TiO$_2$ heat treated at different temperatures (600, 800, 900, and 1000 °C) is obtained to be approximately 20.86, 21.15, 46.11, and 48.53 nm, respectively. As expected, the crystallite size increased with increasing heat treatment temperature. The surface area of the samples heat treated at different temperatures was examined by BET and it was obtained at 60, 58, 45, and 34 m^2 g^{-1} respectively. Raman spectroscopy was used to investigate the carbon coating on the CC-TiO$_2$ heat treated samples at different temperatures and an argon laser of 514 nm was used as the excitation source. We observed a prominent band around 1350 cm^{-1} in all the samples as shown in Fig. 2. This band is known as the D band but the intensity of this band decreases with the increasing heat treatment temperature of the samples. Another prominent band was also observed at 1598 cm^{-1} in all the samples, this is known as the G band and the intensity of this band increases with increasing temperature.[56–59] Two bands were also observed around 403 and 640 cm^{-1} in all the samples, which correspond to TiO$_2$.[52–54] The I_D/I_G ratio was found to be 1.16, 1.05, 1.03, and 0.85 for CC-TiO$_2$ heat treated at 600 °C, 800 °C, 900 °C, and 1000 °C respectively. The I_D/I_G ratio of the CC-TiO$_2$ samples decreases with increasing temperature suggesting that the crystalline nature of the carbon coated on the TiO$_2$ particles improves with increasing temperature.

The morphology of the CC-TiO$_2$ was further studied by FEG-SEM. Fig. 3(a–d) show the morphology of the particles of CC-TiO$_2$. Fig. 3(a) shows the particle size to be around 50 nm. Fig. 3(b–d) show the particles to be irregular and the particle size is up to a few 100 nm suggesting that the particles are agglomerates comprising of the primary crystallites.

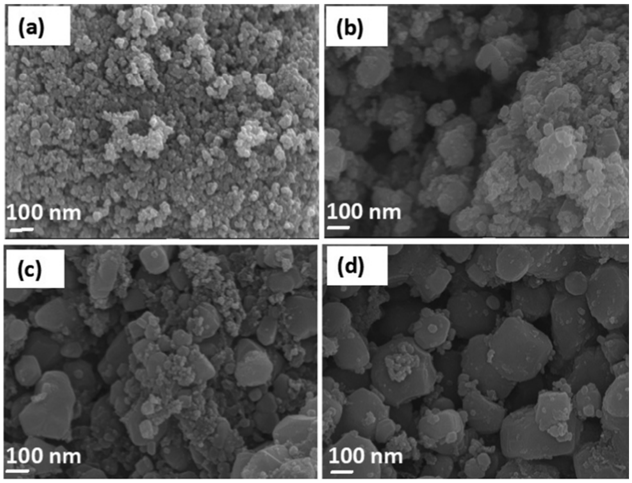

Fig. 3 FEG-SEM micrographs of CC-TiO$_2$ heat treated at different temperatures, (a) 600 °C, (b) 800 °C, (c) 900 °C, and (d) 1000 °C.

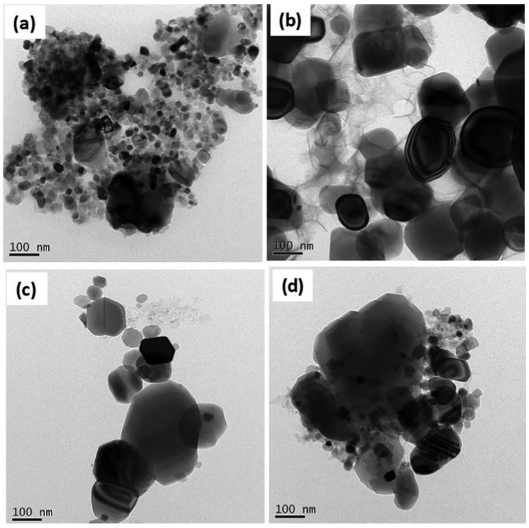

Fig. 4 FEG-TEM micrographs of CC-TiO_2 heat treated at different temperatures, (a) 600 °C, (b) 800 °C, (c) 900 °C, and (d) 1000 °C.

Results from FEG-TEM of CC-TiO_2 are shown in Fig. 4. It can be seen from Fig. 4(a) that the size of most of the particles is less than 30 nm, while it can be observed from Fig. 4(b–d) that the particle size increases with increasing heat treatment temperature. This correlates with the changes in the crystallite and particle size as determined from XRD and FEG-SEM. The transformation of the anatase phase into the rutile phase led to a bigger particle size, higher density and volume shrinkage.[53] As could be seen also by FEG-SEM and FEG-TEM micrographs of these samples, the annealing temperature has a significant impact on the particle size and it increases with increasing temperature. The XRD results are consistent with the FEG-SEM and FEG-TEM results.

3.2. Photocatalyic analysis of CC-TiO_2

The photocatalytic efficiency of CC-TiO_2 samples heat treated at different temperatures was monitored by using cationic dyes MB and CV as model pollutants. The percentage adsorption efficiency of all the samples after 30 minutes for MB and CV dyes is shown by a comparative bar graph in Fig. 5. With an increasing heat treatment temperature of CC-TiO_2, the carbon content on the surface decreases to a certain extent along with the surface area. The sample heat treated at 600 °C has the lowest adsorption efficiency for both the dyes. Furthermore, the percentage adsorption of the two dyes in the case of the sample heat treated at 800 °C was the highest. As seen in the SEM micrographs above, the powder particles obtained by heat treatment at higher temperatures pack poorly possibly allowing better access for the dye molecules to the powder particle (agglomerate) surfaces. The difference in adsorption efficiency may also be linked to uniform coating of the carbon on TiO_2 as well as the presence of mixed phases of TiO_2 *i.e* anatase and rutile. On the other hand, the adsorption efficiency for the 900 °C sample is a little lower than that of the 800 °C sample as the rutile phase started to form at 900 °C and hence the surface area of the particles started to decrease; thus, lowering the percentage adsorption of the pollutant.[60] The percentage adsorption is the lowest for the heat treated sample at 1000 °C for both the dyes due to complete rutile phase formation as compared to other samples.[61] Another reason for the lower adsorption of dyes by the samples treated at a temperature higher than 800 °C is attributed to the decreasing concentration of carbon content on the TiO_2 surface with increasing annealing temperatures.[62]

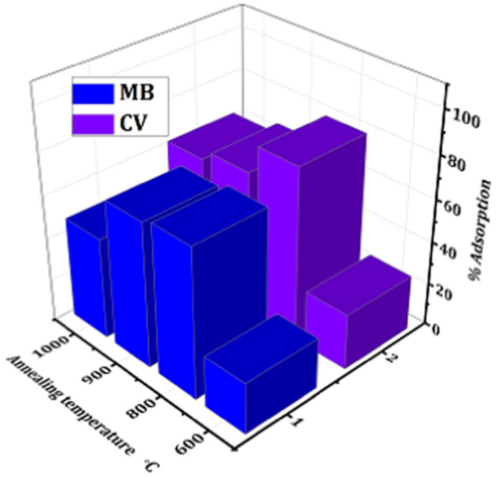

Fig. 5 The comparative bar graph of % adsorption of MB and CV dyes using CC-TiO_2 heat treated at different temperatures (600, 800, 900, and 1000 °C).

The degradation study was carried out under visible light and the data was taken after an interval of 20 minutes. The % degradation with irradiation time comparatively for MB and CV dye using all the samples is shown in Fig. 6. In the case of MB, the % degradation is the highest for the sample heat treated at 800 °C (94.13%), followed by 900 °C (77.14%), 1000 °C (43.08%) and 600 °C (18.94%). Similarly, in the case of CV, the order follows 800 °C (99.72%) > 900 °C (97.14%) > 1000 °C (73.62%) > 600 °C (27.27%). The lower % degradation of dyes by sample treated at 600 °C under visible light irradiation may be attributed to its higher band gap and the presence of carbon with a greater extent of structural defects.[63] The reason for the higher dye degradation efficiency of the sample heat treated at 800 °C

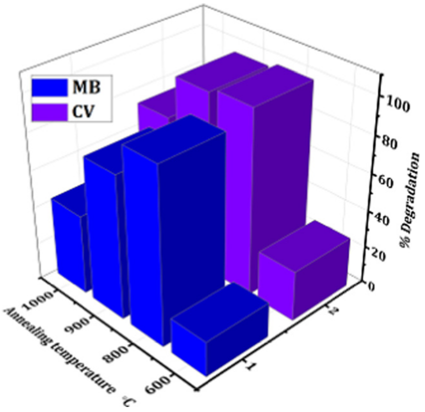

Fig. 6 The comparative bar graph of % degradation of MB and CV dyes using CC-TiO_2 heat treated at different temperatures (600, 800, 900, and 1000 °C).

Table 1 Comparison table of the photocatalytic activity of carbon based TiO_2 materials for MB and CV dyes

Photocatalyst	Dye	Conditions	Material's band gap (eV)	Degradation (%)	Time (min.)	Ratio (material(mg)/dye(mg)) in 1 liter water	Ref.
Nano-composites TiO_2–AC	MB	UV-Light	2.1	95	180	1000/100	67
TiO_2/CSAC	MB	UV-Light		100	60	1000/50	68
TiO_2@C	MB	Visible-light	3.27	100	30	1000/20	69
TiO_2-decorated-CNF	MB	UV-Light	—	100	180	800/6.4	70
TiO_2/graphene porous composites	MB	Visible-light	2.56	95	150	10/10	71
TiO_2-exfoliated graphite oxide	MB	UV-Light	3.10	100	90	500/10	72
Graphene–TiO_2-composites	MB	Visible-light	2.80	94	150	500/10	73
rGO–TiO_2/Co_3O_4 nanocomposite	MB	Visible-light	2.74	90	120	50/10	74
CC-TiO_2	MB	Visible-light	2.95	94	120	100/5	Current work
F-TiO_2(B)/fullerene	CV	Visible-light	2.6	77	120	100/30	75
CNCs–TiO_2 heterojunctions	CV	UV-Light	2.55	60	180	300/10	76
Graphene–Ce–TiO_2	CV	UV-Light	—	59	15	20/60	77
Graphene–Fe–TiO_2	CV	UV-Light	—	75	15	20/60	77
TiO_2-based nanosheet	CV	UV-Light	3.05	45	30	1000/40	78
rGO–TiO_2/Co_3O_4 nanocomposite	CV	Visible-light	2.74	80	120	50/10	74
TiO_2–montmorillonite	CV	UV-Light	—	97	350	160/40.8	79
Nano-TiO_2/Diatomite	CV	UV-Light	—	99	210	25/25	80
CC-TiO_2	CV	Visible-light	2.95	100	60	100/5	Current work

for both dyes is due to lower optical band gap of anatase TiO_2 at a higher annealing temperature. It is chemically and optically active and hence enhances the catalysis process in the dyes.[62,64] The % degradation of sample heat treated at 900 °C is either lower or similar to the sample heat treated at 800 °C, because the rutile phase started to form above 800 °C as confirmed from the XRD results. The complete rutile nature of the sample heat treated at 1000 °C lowers its degradation efficiency as it is less active than the anatase phase. Thus, the results obtained, as shown in Table 1, are in accordance with the reported literature.[65–80]

The plot of C/C_0 *vs.* time for MB and CV using all the synthesized samples are shown in Fig. 7(a and b), respectively. Where, C_0 and C represent the initial solution concentrations ($t = 0$) and the solution concentration at any irradiation time t.

In order to study the degradation kinetics of the photocatalytic reactions, the obtained data were fitted with pseudo first order (PFO) and pseudo second order (PSO) kinetic models. The reactions involved in PFO and PSO can be written as:

$$-\ln\frac{C}{C_0} = K_1 t \qquad \text{(i)}$$

$$\frac{t}{C} = \frac{1}{K_2 {C_0}^2} + \frac{t}{C_0} \qquad \text{(ii)}$$

where C_0, C, K_1 and K_2 represent the initial solution concentrations ($t = 0$), the solution concentration at any irradiation time t, and the PFO & PSO rate constant (min^{-1}), respectively. The plots of PFO ($-\ln(C/C_0)$ *vs.* t (min.)) for MB and CV are represented in Fig. 8(a and c), respectively, and the plots of PSO (t/C *vs.* t (min.)) for MB and CV are shown in Fig. 8(b and d), respectively. The parameters obtained such as rate constant (K_1 and K_2 (min^{-1})) and regression coefficient (R^2) from fitting the data with PFO and PSO are given in Table 2. From the table and fitted data one can observe that sample 600 °C follows the PSO kinetic model, while the 800 °C sample follows the PFO kinetic model on the basis of R^2 values and having the highest K_1 values *i.e.* 0.0234 and 0.0509 for MB and CV, respectively. Similarly, 900 °C also follows the PFO model for both the dyes. Sample 1000 °C follows both the models i.e PFO and PSO for CV and MB, respectively.

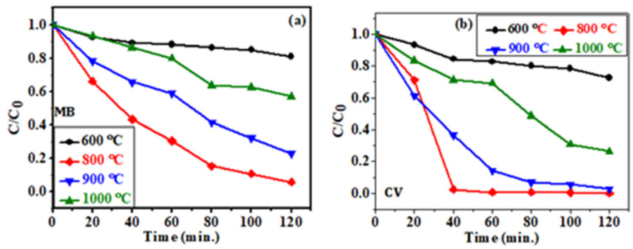

Fig. 7 Change in concentration of (a) MB and (b) CV dye with irradiation time for CC-TiO_2 heat treated at different temperatures (600, 800, 900, and 1000 °C).

3.3. Degradation mechanism of CC-TiO_2

On the basis of the results, Fig. 10 illustrates the degradation mechanism of dyes using the 800 °C sample. With the visible light irradiation, the generation of electron-hole pairs takes place at the surface of CC-TiO_2 when the visible light has an energy greater than or equal to the band gap energy of the catalyst. The anatase TiO_2 has a band gap of nearly 3.2 eV.[63,81] As the heat treatment temperature increases, the size of the nanoparticles also increases and leads to lowering the band gap of the materials. This has been well reported in the literature.[64,82] The optical band gap of CC-TiO_2 heat treated at different temperatures is shown in Fig. 9. It is found to be 3.25, 2.95, 3.03 and 3.06 eV for samples heat treated at temperatures of 600, 800, 900, and 1000 °C, respectively. The optical band gap of CC-TiO_2 is minimum (2.95 eV) when the sample is heat treated at 800 °C. The reduced optical band gap materials have a higher absorption of visible light generating higher electron–hole pairs. The quick recombination of electron–hole pairs will lead to suppression of the photocatalytic activity. Thus, it is important to quench the recombination of charge pairs for efficient photocatalysis.

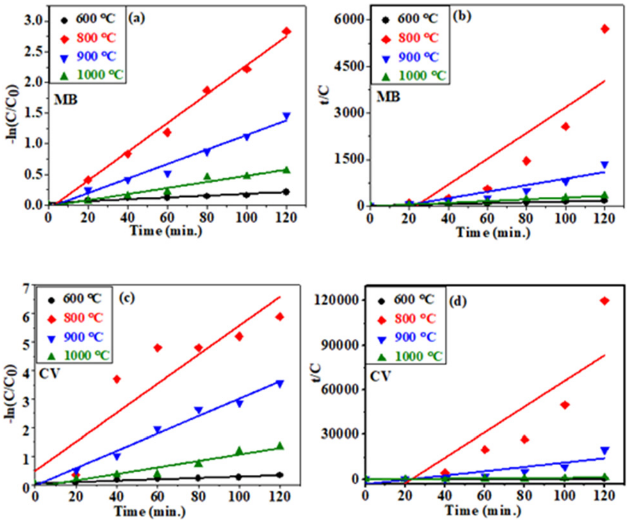

Fig. 8 The PFO (a and c) and PSO (b and d) kinetics of the degradation of MB and CV dye in the presence of CC-TiO$_2$ heat treated at different temperatures (600, 800, 900, and 1000 °C).

Table 2 Parameters obtained from PFO and PSO kinetics

Dye	Catalyst (°C)	K_1 (min^{-1})	R^2	K_2 (min^{-1})	R^2
MB	600	0.0014	0.902	0.5675	0.997
	800	0.0234	0.991	1.7693	0.709
	900	0.0118	0.974	0.6106	0.843
	1000	0.0049	0.957	0.3391	0.974
CV	600	0.0024	0.933	0.4379	0.992
	800	0.0509	0.816	36.956	0.701
	900	0.0304	0.983	5.9938	0.700
	1000	0.0113	0.930	0.5171	0.857

Here, the carbon coating on the surface of TiO$_2$ plays an important role and captures the electrons in the conduction band of TiO$_2$. These electrons will further react with the oxygen molecule (O$_2$) to form superoxide anion radicals (O$_2^{\bullet -}$) and the holes in the valence band react with the water to produce a hydroxyl radical [$^{\bullet}$OH]. These ions will further react with the dye molecules adsorbed on the surface to form degradation products such as CO$_2$ and water. The mechanism as proposed has been shown in Fig. 10.

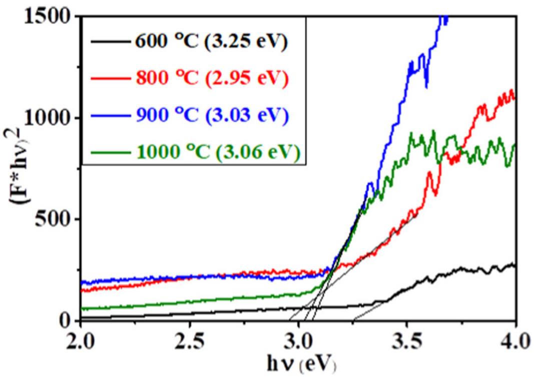

Fig. 9 Tauc plot for CC-TiO$_2$ heat treated at different temperatures (600, 800, 900, and 1000 °C).

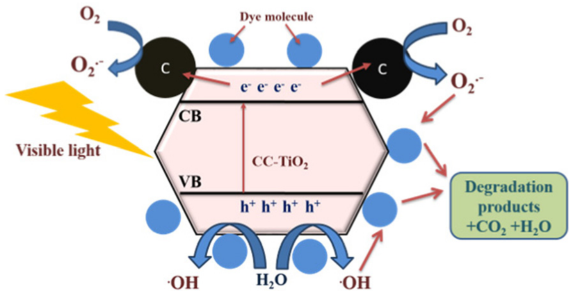

Fig. 10 Proposed mechanism for the degradation of dye molecules.

4. Conclusions

A new approach to fabricate carbon coated-TiO$_2$ nanoparticles is used. CC-TiO$_2$ is synthesized using TiO$_2$ and sucrose, followed by subsequent heat treatment at different temperatures in an argon atmosphere. Carbon coating on titanium dioxide enhances the specific surface area and prevents agglomeration of nanoparticles effectively as indicated by the significant retention of specific surface area even at temperatures as high as 1000 °C. The complete phase transformation from anatase to rutile occurred at high temperatures above 900 °C. The best photocatalytic activity under visible light is observed for the sample heat treated at 800 °C for MB (94. 13% K_1 = 0.0234 min^{-1}) and CV (99.72%, K_1 = 0.0509 min^{-1}), respectively. The carbon coated mixed anatase and rutile phase containing sample is the most efficient photocatalyst. The proposed route is a promising way to synthesize cheap and efficient visible light photocatalysts for harmful organic dye degradation.

Conflicts of interest

There are no conflicts to declare.

Acknowledgements

Dr. R. Kumar acknowledges the financial support received from the Department of Science and Technology-Science and Engineering Board (DST-SERB) through the National Post-Doctoral Fellowship by the Government of India (PDF/2018/001656). The authors are grateful to the Sophisticated Analytical Instrument Facility (SAIF), IIT Bombay, for the characterization facilities.

References

1 A. Fujishima and K. Honda, Electrochemical photolysis of water at a semiconductor electrode, *Nature*, 1972, **238**, 37–38.
2 A. Kudo and M. Miseki, Heterogeneous photocatalyst materials for water splitting, *Chem. Soc. Rev.*, 2009, **38**, 253–278.

3 R. Wang, K. Hashimoto, A. Fujishima, M. Chikuni, E. Kojima, A. Kitamura, M. Shimohigoshi and T. Watanabe, *Nature*, 1977, **388**, 431.

4 K. Hashimoto, H. Irie and A. Fujishima, TiO_2 Photocatalysis: A Historical Overview and Future Prospects, *Jpn. J. Appl. Phys.*, 2005, **44**, 8269–8285.

5 T. V. Gerven, G. Mul, J. Moulijn and A. Stankiewicz, A review of intensification of photocatalytic processes, *Chem. Eng. Process.*, 2007, **46**, 781–789.

6 M. Inagaki, F. Kojin, B. Tryba and M. Toyoda, Carbon-coated anatase: the carbon layer for photocatalytic performance, *Carbon*, 2005, **43**, 1652–1659.

7 K. Lee, H. Yoon, C. Ahn, J. Park and S. Jeon, Strategies to improve the photocatalytic activity of TiO_2: 3D nanostructuring and heterostructuring with Graphitic Carbon Nanomaterials, *Nanoscale*, 2019, **11**, 7025–7040.

8 D. Mitoraj and H. Kisch, The Nature of Nitrogen-Modified Titanium Dioxide Photocatalysts Active in Visible Light, *Angew. Chem., Int. Ed.*, 2008, **47**, 9975–9978.

9 J. Schneider, M. Matsuoka, M. Takeuchi, J. Zhang, Y. Horiuchi, M. Anpo and D. W. Bahnemann, Understanding TiO_2 Photocatalysis: MechanismsandMaterials, *Chem. Rev.*, 2014, **114**, 9919–9986.

10 M. A. Fox, C. C. Chen, K. Park and J. N. Younathan, In Organic Transformations in Non-Homogeneous Media, *ACS Symp. Ser.*, 1985, 278.

11 Z. Jiang, Q. Chen, Q. Zheng, R. Shen, P. Zhang and X. Li, Constructing 1D/2D Schottky-Based Heterojunctions between Mn0.2Cd0.8S Nanorods and Ti_3C_2 Nanosheets for Boosted Photocatalytic H_2 Evolution, *Acta Phys. -Chim. Sin.*, 2021, **37**(6), 2010059.

12 R. He, R. Chen, J. Luo, S. Zhang and D. Xu, Fabrication of Graphene Quantum Dots Modified BiOI/PAN Flexible Fiber with Enhanced Photocatalytic Activity, *Acta Phys. -Chim. Sin.*, 2021, **37**(6), 2011022.

13 X. Li, J. Liu, J. Huang, C. He, Z. Feng, Z. Chen, L. Wan and F. Deng, All Organic S-Scheme Heterojunction PDI-Ala/S-C_3N_4 Photocatalyst with Enhanced Photocatalytic Performance, *Acta Phys. -Chim. Sin.*, 2021, **37**(6), 2010030.

14 J. Pan, Z. Guan, J. Yang and Q. Li, Facile fabrication of $ZnIn_2S_4$/SnS_2 3D heterostructure for efficient visible-light photocatalytic reduction of Cr(VI), *Chin. J. Catal.*, 2020, **41**, 200–208.

15 R. Shen, Y. Ding, S. Li, P. Zheng, Q. Xiang, Y. H. Ng and X. Li, Constructing low-cost Ni_3C/twin-crystal $Zn_{0.5}Cd_{0.5S}$ heterojunction/homojunction nanohybrids for efficient photocatalytic H_2 evolution, *Chin. J. Catal.*, 2021, **42**, 25–36.

16 J. Wang, G. Wang, B. Cheng, J. Yu and J. Fan, Sulfur-doped g-C_3N_4/TiO_2 S-scheme heterojunction photocatalyst for Congo Red photodegradation, *Chin. J. Catal.*, 2021, **42**, 56–68.

17 X. Li, Y. Deng, Z. Jiang, R. Shen, J. Xie, W. Liu and X. Chen, Photocatalytic Hydrogen Production over CdS Nanomaterials: An Interdisciplinary Experiment for Introducing Undergraduate Students to Photocatalysis and Analytical Chemistry, *Chem. Educ.*, 2019, **96**, 1224–1229.

18 Y. Li, M. Zhou, B. Cheng and Y. Shao, Recent advances in g-C_3N_4-based heterojunction photocatalysts, *J. Mater. Sci. Technol.*, 2020, **56**, 1–17.

19 R. Shen, D. Ren, Y. Ding, Y. Guan, Y. H. Ng, P. Zhang and X. Li, Nanostructured CdS for efficient photocatalytic H_2 evolution: A review, *Sci. China Mater.*, 2020, **63**(11), 2153–2188.

20 D. Ren, W. Zhang, Y. Ding, R. Shen, Z. Jiang, X. Lu and X. Li, In-situ fabricating robust cocatalyst-free CdS/g-C_3N_4 2D-2D step-scheme heterojunctions for highly active H_2 evolution, *Sol. RRL*, 2020, **4**, 1900423.

21 R. Shen, X. Lu, Q. Zheng, Q. Chen, Y. H. Ng, P. Zheng and X. Li, Tracking S-Scheme Charge Transfer Pathways in Mo_2C/CdS H_2-Evolution Photocatalysts, *Sol. RRL*, 2021, 2100177.

22 R. Leary and A. Westwood, Carboneous nanomaterials for the enhancement of TiO_2 photocatalysis, *Carbon*, 2011, **49**, 741–772.

23 N. R. Khalid, A. Majid, M. B. Tahir, N. A. Naiz and S. Khalid, Carbonaceous-TiO_2 nanomaterials for photocatalytic degradation of pollutants: A review, *Ceram. Int.*, 2017, **43**, 14552–14571.

24 J. Zhang, M. Vasei, Y. Sang, H. Liu and J. P. Claverie, TiO_2@Carbon Photocatalysts: The Effect of Carbon Thickness on Catalysis, *ACS Appl. Mater. Interfaces*, 2016, **8**, 1903–1912.

25 K. Palanivelu, J. S. Im and Y. S. Lee, Carbon doping of TiO_2 for visible light photocatalysis – A review, Carbon, *Science*, 2007, **3**, 214–224.

26 H. Zhang, X. Lv, Y. Li, Y. Wang and J. Li, P25-graphene composite as a high performance photocatalyst, *ACS Nano*, 2010, **4**, 380–386.

27 S. D. Perera, R. G. Mariano, K. Vu, N. Nour, O. Seitz, Y. Chabal and K. J. Balkus, Hydrothermal synthesis of graphene-TiO_2 nanotube composites with enhanced photocatalytic activity, *ACS Catal.*, 2012, **2**, 949–956.

28 P. V. Kamat, Graphene-based nanoassemblies for energy conversion, *J. Phys. Chem. Lett.*, 2011, **2**, 242–251.

29 Y. Zhang, Z.-R. Tang, X. Fu and Y.-J. Xu, TiO2–graphene nanocomposites for gasphase photocatalytic degradation of volatile aromatic pollutant: is TiO2–graphene truly different from other TiO_2–carbon composite materials, *ACS Nano*, 2010, **4**, 7303–7314.

30 W. Fan, Q. Lai, Q. Zhang and Y. Wang, Nanocomposites of TiO2 and reduced graphene oxide as efficient photocatalysts for hydrogen evolution, *J. Phys. Chem. C*, 2011, **115**, 10694–10701.

31 Y. T. Liang, B. K. Vijayan, K. A. Gray and M. C. Hersam, Minimizing graphene defects enhances titania nanocomposite-based photocatalytic reduction of CO_2 for improved solar fuel production, *Nano Lett.*, 2011, **11**, 2865–2870.

32 H. Gao, X. Li, J. Lv and G. Liu, Interfacial charge transfer and enhanced photocatalytic mechanisms for the hybrid graphene/anatase TiO_2(001) nanocomposites, *J. Phys. Chem. C*, 2013, **117**, 16022–16027.

33 W. Ren, Z. Ai, F. Jia, L. Zhang, X. Fan and Z. Zou, Low temperature preparation and visible light photocatalytic activity of mesoporous carbon doped crystalline TiO_2, *Appl. Catal., B*, 2007, **69**, 138–144.

34 X. Lin, F. Rong, X. Ji and D. Fu, Carbon-doped mesoporous TiO_2 film and its photocatalytic activity, *Microporous Mesoporous Mater.*, 2011, **142**, 276–281.

35 R. Kumar, B. K. Singh, A. Soam, S. Parida, V. Sahajwalla and P. Bhargava, In-situ carbon supported titanium dioxide (ICS-TiO_2) as electrode material for high performance supercapacitors, *Nanoscale Adv.*, 2020, **2**, 2376–2386.

36 H. Park and H.-I. Kim, G.-h. Moon, W. Choi, Photoinduced charge transfer processes in solar photocatalysis based on modified TiO_2, *Energy Environ. Sci.*, 2016, **9**, 411–433.

37 J. Shi, On the synergetic catalytic effect in heterogeneous nanocomposite catalysts, *Chem. Rev.*, 2013, **113**, 2139–2181.

38 B. Neumann, P. Bogdanoff, H. Tributsch, S. Sakthivel and H. Kisch, Electrochemical mass spectroscopic and surface photovoltage studies of catalytic water photooxidation by undoped and carbon-doped titania, *J. Phys. Chem. B*, 2005, **109**, 16579–16586.

39 L. Zhang, M. S. Tse, O. K. Tan, Y. X. Wang and M. Han, Facile fabrication and characterization of multi-type carbon-doped TiO_2 for visible light-activated photocatalytic mineralization of gaseous toluene, *J. Mater. Chem. A*, 2013, **1**, 4497–4507.

40 G. Zhang, F. Teng, Y. Wang, P. Zhang, C. Gong, L. Chen, C. Zhao and E. Xie, Preparation of carbon–TiO_2 nanocomposites by a hydrothermal method and their enhanced photocatalytic activity, *RSC Adv.*, 2013, **3**, 24644–24649.

41 A. C. Pierre, *Introduction to sol-gel processing*, Boston: Kluwer Academic Publishers; 1998.

42 K. Byrappa and M. Yoshimura, *Hand book of hydrothermal technology: a technology for crystal growth and materials processing*, Norwich, NY: Noyes Publcations, William Andrew Publishing: 2001.

43 K. Reichelt and X. Jiang, The prepration of thin films by physical vapour deposition methods, *Thin Solid Films*, 1990, **191**, 91–126.

44 D. M. Dobkin and M. K. Zuraw, *Pricniples of chemical vapour deposition*, The Netherlands: Kluwer Academic Press; 2003.

45 O. Vander, Biest, Electrophoretic deposition of materials, *Annu. Rev. Mater. Sci.*, 1999, **29**, 356–372.

46 R. Kumar and P. Bhargava, Synthesis and Characterization of low specific resistance alumina-clay-carbon composites by colloidal processing using sucrose as a soluble carbon source for electrical applications, *RSC Adv.*, 2016, **6**, 8705–8713.

47 R. Kumar, A. Soam and V. Sahajwalla, Sucrose-derived carbon-coated nickel oxide (SDCC-NiO) as an electrode material for supercapacitor applications, *Mater. Adv.*, 2020, **1**, 609–616.

48 R. Kumar and P. Bhargava, Fabrication of low specific resistance ceramic carbon composites by slip casting, *Asian Ceram. Soc.*, 2015, **3**, 262–265.

49 R. Kumar and R. K. Nekouei, Veena Sahajwalla, In-situ carbon-coated tin oxide (ISCC-SnO_2) for micro-supercapacitor applications, *Carbon Lett.*, 2020, **30**, 699–707.

50 Y. Q. Hou, D. M. Zhuang, G. Zhang, M. Zhao and M. S. Wu, Influence of annealing temperature on the properties of titanium oxide thin film, *Appl. Surf. Sci.*, 2003, **218**, 97–105.

51 D. A. H. Hanaor and C. C. Sorrell, Review of the anatase to rutile phase transformation, *J. Mater. Sci.*, 2011, **46**, 855–874.

52 Y. Sun, T. Egawa, L. Zhang and X. Yao, High anatase-rutile transformation temperature of anatase titania nanoparticles prepared by metalorganic chemical vapor deposition, *Jpn. J. Appl. Phys.*, 2002, **41**, L945–L948.

53 J. M. G. Amores, V. S. Escribano and G. Busca, Anatase crystal growth and phase transformation to rutile in high area TiO_2, MOO,-TiO, and Other TiO,-supported oxide catalytic systems, *J. Mater. Chem.*, 1995, **5**, 1245–1249.

54 B. Xia, H. Huang and Y. Xie, Heat treatment on TiO_2 nanoparticles prepared by vapor-phase hydrolysis, *Mater. Sci. Eng., B*, 1999, **57**, 150–154.

55 Y. Zhong, C. K. Chan, J. F. Porter and W. Guo, Micro-Raman spectroscopic characterization of nanosized TiO_2 powders prepared by vapor hydrolysis, *J. Mater. Res.*, 1998, **13**, 2602–2609.

56 R. Kumar, A. Soam, R. O. Dusane and P. Bhargava, Sucrose derived carbon coated silicon nanowires for supercapacitor application, *J. Mater. Sci.: Mater. Electron.*, 2018, **29**, 1947–1954.

57 R. Kumar, V. Sahajwalla and P. Bhargava, Fabrication of a counter electrode for dye-sensitized solar cells (DSSCs) using carbon material produced by organic ligand 2-Methyl- 8-hydroxyquinolinol (Mq), *J. Nanoscale Adv.*, 2019, **1**, 3292–3299.

58 R. Kumar, A. Raj, S. Mitra and P. Bhargava, Carbon derived from sucrose as anode material for lithium-ion batteries, *J. Electron. Mater.*, 2019, **48**, 7389–7395.

59 R. Kumar, A. Soam, R. Hussian, I. Mansuri and V. Sahajwalla, Carbon coated iron oxide (CC-IO) as high performance electrode material for supercapacitor applications, *J. Energy Storage*, 2020, **32**, 101737.

60 D. A. H. Hanaor and C. C. Sorrell, Review of anatase to rutile phase transformation, *J. Mater. Sci.*, 2011, **46**, 855–874.

61 K. N. P. Kumar, K. Kerzer and A. J. Burggraaf, Stabilization of the porous texture of nanostructured titania by avoiding a phase transformation, *J. Mater. Sci. Lett.*, 1994, **13**, 59–61.

62 Z. Jiang, H. Zheng-hong, X. Yong and K. Fei-yu, Carbon-coated TiO_2 composites for the photocatalytic degradation of low concentration benzene, *New Carbon Mater.*, 2011, **26**, 63–70.

63 S. Banerjee, S. C. Pillai, P. Falaras, K. E. O'Shea, A. J. Byrne and D. D. Dionysiou, New Insights into the Mechanism of Visible Light Photocatalysis, *J. Phys. Chem. Lett.*, 2014, **5**, 2543–2554.

64 S. Mathur, M. Arya, R. Jain and S. K. Sharma, Effect of Annealing Temperature on Structural, Electrical and Optical Properties of TiO_2 Nanopowder, *J. Nanostruct.*, 2017, **7**, 121–126.

65 B. Xia, H. Huang and Y. Xie, Heat treatment on TiO_2 nanoparticles prepared by vapor-phase hydrolysis, *Mater. Sci. Eng., B*, 1999, **57**, 150–154.

66 Y. Zhong, C. K. Chan, J. F. Porter and W. Guo, Micro-Raman spectroscopic characterization of nanosized TiO_2 powders prepared by vapor hydrolysis, *J. Mater. Res.*, 1998, **13**, 2602–2609.

67 R. A. El-Salamony, E. Amdeha, S. A. Ghoneim, N. A. Badawy, K. M. Salem and A. M. Al-Sabagh, Titania Modified

Activated Carbon Prepared from Sugar Cane Bagasse: Adsorption and Photocatalytic Degradation of Methylene Blue under Visible Light Irradiation, *Environ. Technol.*, 2017, **38**, 3122–3136.

68 H. A. Le, L. T. Linh, S. Chin and J. Jurng, Photocatalytic degradation of methylene blue by a combination of TiO_2-anatase and coconut shell activated carbon, *Power Technol.*, 2012, **225**, 167–175.

69 X. Gao, P.-G. Rena, J. Wang, F. Rena, Z. Dai and Y.-L. Jin, Fabrication of visible-light responsive TiO2@C photocatalyst with an ultrathin carbon layer to efficiently degrade organic pollutan, *Appl. Surf. Sci.*, 2020, **532**, 147482.

70 H. Wang, X. Huang, W. Li, J. Gao, H. Xue, R. K. Y. Li and Y. W. Mai, TiO_2 nanoparticle decorated carbon nanofibers for removal of organic dyes, *Colloids Surf., A*, 2018, **549**, 205–211.

71 Y. Yang, L. Xu, H. Wang, W. Wang and L. Zhang, TiO_2/graphene porous composite and its photocatalytic degradation of methylene blue, *Mater. Des.*, 2016, **108**, 632–639.

72 V. Z. Baldissarelli, T. d Souza, L. Andrade, L. F. C. Oliveira, H. J. José and R. d F. P. M. Moreira, Preparation and photocatalytic activity of TiO_2-exfoliated graphite oxide composite using an ecofriendly graphite oxidation method, *Appl. Surf. Sci.*, 2015, **359**, 868–874.

73 S. Liu, H. Sun, S. Liu and S. Wang, Graphene facilitated visible light photodegradation of methylene blue over titanium dioxide photocatalysts, *Chem. Eng. J.*, 2013, **214**, 289–303.

74 R. Ranjith, V. Renganathan, S.-M. Chen, N. Senthamizh Selvana and P. Shameel Rajam, Green synthesis of reduced graphene oxide supported TiO_2/Co_3O_4 nanocomposite for photocatalytic degradation of methylene blue and crystal violet, *Ceram. Int.*, 2019, **45**, 12926–12933.

75 Y. Panahian, N. Arsalani and R. Nasiri, Enhanced photo and sono-photo degradation of crystal violet dye in aqueous solution by 3D flower like F-TiO_2(B)/fullerene under visible light, *J. Photochem. Photobiol., A*, 2018, **365**, 45–51.

76 Q. Wu, H. Yang, H. Zhu and Z. Gao, Construction of CNCs-TiO_2 heterojunctions with enhanced photocatalytic activity for crystal violet removal, *Optik*, 2019, **179**, 195–206.

77 T. P. Shende, B. A. Bhanvase, A. P. Rathod, D. V. Pinjari and S. H. Sonawane, Sonochemical synthesis of Graphene-Ce-TiO_2 and Graphene-Fe-TiO_2 ternary hybrid photocatalyst nanocomposite and its application in degradation of crystal violet dye, *Ultrason. Sonochem.*, 2018, **41**, 582–589.

78 F. Chen, P. Fang, Y. Gao, Z. Liu, Y. Liu and Y. Dai, Effective removal of high-chroma crystal violet over TiO_2-based nanosheet by adsorption–photocatalytic degradation, *Chem. Eng. J.*, 2012, **204–206**, 107–113.

79 R. Djellabi, M. F. Ghorab, G. Cerrato, S. Morandi, S. Gatto, V. Oldani, A. Di Michele and C. L. Bianchi, Photoactive TiO_2–montmorillonite composite for degradation of organic dyes in water, *J. Photochem. Photobiol., A*, 2014, **295**, 57–63.

80 R. Cherrak, M. Hadjel, N. Benderdouche, M. Adjdir, A. Mokhtar, K. Khaldi, A. Sghier and P. G. Weidler, Preparation of Nano-TiO_2/Diatomite Composites by Non-hydrolytic Sol–Gel Process and its Application in Photocatalytic Degradation of Crystal Violet, *Silicon*, 2020, **12**, 927–935.

81 P. Singla, O. P. Pandey and K. Singh, Study of Photocatalytic degradation of environmentally harmful phthalate esters using Ni-doped TiO_2 nanoparticles, *Int. J. Environ. Sci. Technol.*, 2016, **13**, 849–856.

82 P. Singla, M. Sharma, O. P. Pandey and K. Singh, Photocatalytic degradation of azo dyes using Zn-doped and undoped TiO_2 nanoparticles, *Appl. Phys. A: Mater. Sci. Process.*, 2013, **116**, 371–378.